Large-Scale Retrieval and Quality Control of Leaf Area Index Based on ICESat-2 Spaceborne Photon-Counting Laser Altimeter

Da Guo, Xiaoning Song, *Member, IEEE*, Ronghai Hu, *Senior Member, IEEE*, Max Mallen-Cooper, Yuzhen Xing, Ruijin Li, Hong Zeng, Han Guo, Guangjian Yan, *Senior Member, IEEE*, and Paul Kardol

Abstract*—Spaceborne light detection and ranging (LiDAR) provides a promising method for large-scale characterizing leaf area index (LAI). However, the quality of point cloud data from spaceborne LiDAR, especially Ice, Cloud, and land Elevation Satellite-2 (ICESat-2), is susceptible to atmosphere and background noise, introducing considerable uncertainty in LAI retrieval. Thus, efficiently screening out the high-quality point cloud is a significant guarantee for high-quality LAI retrieval. In this study, we proposed a quality control (QC) method that employed the number of 10-m windows without ground points in the ICESat-2 100-m segment as the QC flag. This method divided segments into 11 QC flags from 0 to 10 and was applied to LAI retrieval across Chinese forests from 2019 to 2020. The field measurements at locations identical to ICESat-2 ground tracks were used to validate the ICESat-2 LAI at different QC flags. The results showed that the proposed method effectively improved point cloud quality recognition and LAI accuracy, with ICESat-2 LAI (QC <3) reducing root mean square error (RMSE) by 26.36% compared with all ICESat-2 LAIs. It also showed good agreement with Moderate Resolution Imaging Spectroradiometer (MODIS) and Global Land Surface Satellite (GLASS) LAI and mitigated saturation issues in passive optical imagery. The ICESat-2 LAI with QC <3 performed better in deciduous broadleaved, evergreen needle-leaved, deciduous needle-leaved, and mixed forests (MFs), but not in evergreen broadleaved forests (EBFs). ICESat-2 LAI was particularly adept at capturing high-LAI values, which had the highest proportion of LAI values over 6.0 compared with MODIS and GLASS LAI. The proposed method has the potential for large-scale and high-quality LAI retrieval using ICESat-2 data on a global scale.

***Index Terms*—Clumping index (CI), forest leaf area index (LAI), Ice, Cloud, and land elevation Satellite-2 (ICESat-2), large scale, quality control (QC).**

Received 19 October 2024; revised 14 January 2025 and 19 May 2025; accepted 16 July 2025. Date of publication 24 July 2025; date of current version 15 August 2025. This work was supported in part by the National Natural Science Foundation of China under Grant 42271393; in part by the Third Xinjiang Scientific Expedition Program under Grant 2022xjkk0402; in part by the Youth Innovation Promotion Association, Chinese Academy of Sciences (CAS); in part by the Fundamental Research Funds for the Central Universities; in part by the Xiaomi Young Scholar Program; and in part by European Research Council (ERC) under European Union's Horizon 2020 Research and Innovation Program under Grant 864287—THRESHOLD—ERC-2019-COG. *(Da Guo and Xiaoning Song are co-first authors.) (Corresponding author: Ronghai Hu.)*

Da Guo is with the College of Resources and Environment, University of Chinese Academy of Sciences, Beijing 101408, China, also with the Beijing Yanshan Earth Critical Zone National Research Station, University of Chinese Academy of Sciences, Beijing 101408, China, also with the State Key Laboratory of Earth System Numerical Modeling and Application, University of Chinese Academy of Sciences, Beijing 101408, China, and also with the Department of Forest Ecology and Management, Swedish University of Agricultural Sciences, 90183 Umeå, Sweden (e-mail: guoda181@mails.ucas.edu.cn).

Xiaoning Song, Ronghai Hu, Yuzhen Xing, Ruijin Li, Hong Zeng, and Han Guo are with the College of Resources and Environment, University of Chinese Academy of Sciences, Beijing 101408, China, also with the Beijing Yanshan Earth Critical Zone National Research Station, University of Chinese Academy of Sciences, Beijing 101408, China, and also with the State Key Laboratory of Earth System Numerical Modeling and Application, University of Chinese Academy of Sciences, Beijing 101408, China (e-mail: songxn@ucas.edu.cn; huronghai@ucas.edu.cn; xingyuzhen20@mails.ucas.ac.cn; liruijin23@mails.ucas.ac.cn; zenghong211@mails.ucas.ac.cn; guohan221@mails.ucas.ac.cn).

Max Mallen-Cooper and Paul Kardol are with the Department of Forest Ecology and Management, Swedish University of Agricultural Sciences, 90183 Umeå, Sweden (e-mail: maxmallencooper@gmail.com; paul.kardol@slu.se).

Guangjian Yan is with the State Key Laboratory of Remote Sensing Science, Faculty of Geographical Science, Beijing Normal University, Beijing 100875, China (e-mail: gjyan@bnu.edu.cn).

This article has supplementary downloadable material available at https://doi.org/10.1109/TGRS.2025.3592523, provided by the authors.

Digital Object Identifier 10.1109/TGRS.2025.3592523

I. Introduction

FORESTS play a vital role in carbon sequestration, and the 3-D structure of forests contributes significantly to the biodiversity and functioning of terrestrial ecosystems [1], [2], [3]. The horizontal and vertical distribution of forest canopy directly affect radiation interception, the net carbon uptake, and the ability of forests to sustain ecosystem services [4], [5]. Therefore, accurate observations of variations in the spatial structure of forest canopy provide essential baseline data for forest management and carbon modeling.

Leaf area index (LAI) is commonly used to quantify forest canopy structure, which represents one half of the total green leaf area per unit ground surface area [6], [7]. Accurate measurements of LAI on a large scale can provide essential ecological parameters for global plant photosynthesis modeling and carbon accounting [8], [9], [10]. Remote sensing provides various methods for measuring the global LAI, and several LAI products have been developed using passive optical satellite data [11], [12], [13], [14], which have been widely used to study spatiotemporal dynamics of vegetation and greening trends [15], [16], [17], [18], [19]. However, the accuracy of LAI derived from passive optical satellite data is significantly impaired in regions with dense forest canopies, where LAI is very high [20], [21]. Spaceborne light detection and ranging (LiDAR) has the ability to acquire information on both the vertical and horizontal forest canopy information and has been shown to be effective in penetrating the canopy [22], [23]. Therefore, spaceborne LiDAR presents

a good opportunity to improve the accuracy of global forest LAI estimation. Some studies have estimated the forest LAI using the Ice, Cloud, and land Elevation Satellite-2 (ICESat-2) [21], [24], [25], [26], [27], [28] and Global Ecosystem Dynamics Investigation (GEDI) [29], [30], [31], [32], which have made markable progress in using spaceborne LiDAR to retrieve large scale LAI. Notably, ICESat and GEDI are full-waveform LiDAR systems, and the diameter of their footprints is 60 m [33] and 25 m [31], respectively, which are wider than ICESat-2 (11 m) [34]. As the successor of ICESat, ICESat-2 employs a novel photon-counting LiDAR system and can acquire fine spatial resolution and continuous samples along the flight track. Many studies have focused on improving the accuracy of forest parameters estimation using ICESat-2, such as canopy height [35], [36], aboveground biomass [37], [38], [39], and canopy cover [34], [40]. However, there are few studies focused on improving the accuracy of large-scale forest LAI retrieval based on ICESat-2.

As spaceborne LiDAR systems continue to gather more data in forest areas, the study of forest LAI has significantly increased in recent years. Many studies utilized Beer's law to retrieve effective LAI without considering the foliage clumping effect in the canopy [24], [31], [41]. Effective LAI is lower than actual LAI, and some studies demonstrated that foliage aggregation could cause the bias of LAI up to 70% due to the clumping effect [7], [42]. Several methods have been proposed to correct the clumping effect and improve the accuracy of LAI retrieval from spaceborne LiDAR through passive optical satellite data to provide leaves clumping information [21], [25], which would accumulate bias because of different sensors. Jiang et al. [30] corrected the clumping effect by GEDI based on virtual scenes, but the application of this method in actual forest scenes is limited. In addition, it is worth noting that these studies have primarily focused on spaceborne full-waveform LiDAR, with less attention given to clumping effect correction and improving the accuracy of LAI retrieval from photon-counting LiDAR such as ICESat-2. Although Guo et al. [43] have successfully employed a segment-based path length distribution method to retrieve LAI using ICESat-2 on a regional scale, it has not been tested for the inversion of LAI on a large scale.

ICESat-2 is susceptible to solar background noise, and its raw data contains a large amount of ambient noise [44], [45], which has become an important issue affecting the accuracy of large-scale LAI inversion by ICESat-2. Guo et al. [43] found that the good quality of point clouds from ICESat-2 data could improve the accuracy of LAI retrieval. Although the ICESat-2 science team has already done denoise and height normalization (the process of converting the absolute elevation of LiDAR points (i.e., height above sea level or the ellipsoid) into relative height above the ground surface), there are still some point clouds with poor quality that remain in the processed data, including incomplete height normalization and missing point cloud. These poor-quality point clouds would cause a low amount of ground points and low gap fraction (the ratio of ground points and total points in a certain area) [23], [46], as a result of a large uncertainty of LAI retrieval. Therefore, it is significant to effectively screen out the good quality of point clouds when using ICESat-2 data to retrieve LAI, especially on a large scale.

In this study, we proposed an efficient quality control (QC) method for obtaining high-quality point clouds in order to improve the accuracy of LAI retrieval on a large scale by ICESat-2 data. Our main objectives were to: 1) propose a QC method in recognizing QC flags of point cloud for LAI retrieval by ICESat-2 data; 2) evaluate the feasible of the QC method with ground measurements as reference data; and 3) invert forest LAI on a national scale based on the proposed QC method. To accomplish these objectives, we first compared the ICESat-2 LAI with ground measurements to evaluate the reliability and effectiveness of the proposed QC method in screening out high-quality point cloud data. We then employed the segment-based path length distribution method to retrieve forest LAI on a national scale, which allowed us to refine the LAI estimates based on different levels of point cloud quality.

II. Materials

A. ICESat-2 Data

The ICESat-2 Advanced Topographic Laser Altimeter System (ATLAS) was launched in September 2018, and unlike ICESat and GEDI, ICESat-2 ATLAS utilizes photon-counting technology [47]. In brief, ICESat-2 ATLAS continuously samples transects of canopy structure along the flight track, with approximately 11-m footprints illuminated by a 532-nm photon-counting LiDAR sensor [36]. The interval of each shot is 70 cm along the track direction. ICESat-2 ATLAS is equipped with three pairs of laser beams, with each pair having an interval of 3.3 km in the across-track direction. Each pair has a strong beam and a weak beam. Considering the superior performance of the strong beam in detecting both ground and canopy photons compared to the weak beam [47], we have exclusively selected point cloud data from the strong beam for the retrieval of LAI.

One of the objectives of the ICESat-2 mission is to measure vegetation canopy height and ground elevation. The geolocated photon data (ATL03) serves as the input data for higher level products, including land and vegetation data (ATL08). The ATL03 product provides the longitude, latitude, height, along-track segment ID number (segment_id) of each photon, and the number of photons in a given along-track segment (segment_ph_cnt). In addition, ATL03 classifies each photon event as signal or background photon event and provides a confidence assessment on these classifications. ATL03 provides all other spacecraft or instrument information needed by the higher level products. For example, the ATL03 product is used to generate the land and vegetation height (ATL08), which is processed to remove the noise photons and identify the canopy and ground photons. The ATL08 product provides terrain and canopy height along the flight track at a segment size of 100×11 m [40], [48]. In addition, it offers the longitude and latitude of the central position of each segment, the height of photons above the interpolated land surface, indices of photons tracking back to ATL03, and the classification flag for each photon as either noise, ground, canopy, or top of canopy [49]. According to the purpose of our study, we obtained ATL03 [49] and ATL08 [50] products of release 005 for the entire area of China from the National Snow and Ice Data Center

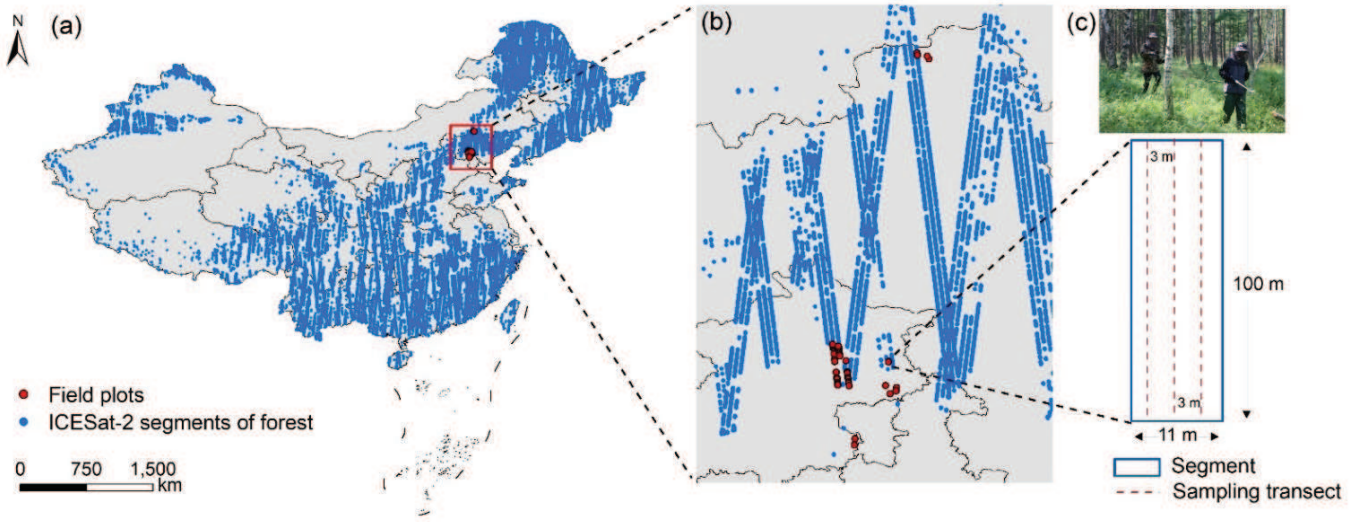

Fig. 1. (a) ICESat-2 spatial trajectories in 2019, (b) locations of the field plots, and (c) field measurements in the 100 × 11 m segment.

(https://nsidc.org) for the period April–October in the years 2019 and 2020.

The indices of photons tracking back to ATL03 were used to trace back to the corresponding ATL03 data within the 100-m segment in order to acquire the photons with relative height (above the ground) and location information (longitude and latitude). Each ATL08 segment was then generated based on the central coordinates provided by ATL08 products. In addition, we applied a land-cover filtering process to select only those ATL08 segments located within the forested ecozone. Fig. 1(a) illustrates the spatial pattern of ATL08 segments in Chinese forests in 2019, with the segments being represented as points using the central coordinates.

B. Ground Plot Data

The ground measurements of LAI were conducted in the northern region of China during the summer of 2021 and 2022. We established 117 sample plots of 100 × 11 m with spatially coincident ATL08 segments [see Fig. 1(b)]. We developed a protocol to obtain ground LAI measurements along the transect (~100 m) at each site using digital cover photography (DCP) according to the characteristics of ICESat-2 along-track records. The cross interval of each transect was approximately 3 m [see Fig. 1(c)]. DCP is an emerging indirect method to measure LAI, utilizing a narrow field of view at the zenith to provide high-resolution images [51]. The camera used for image acquisition had a field of view of 80° and a focal-length lens (in 35-mm format) of 26 mm. For our study, we adopted the path length distribution method proposed by Hu et al. [42] to retrieve the LAI from DCP. With the gap probability obtained from DCP, we used the sliding window to invert the path length distribution from the measured gap data [42].

C. Land-Cover Data

The global 30-m land-cover classification product (GLC_FCS30) from Zhang et al. [52] was acquired from CASEarth (https://data.casearth.cn), which had a spatial resolution of 30 m and a temporal resolution of five years. The forest types of GLC_FCS30 in China include evergreen broadleaved forest (EBF), deciduous broadleaved forest (DBF), evergreen needle-leaved forest (ENF), deciduous needle-leaved forest (DNF), and mixed forest (MF). We used the land-cover product of 2020 to select only forest segments from ICESat-2 ATL08 data in China. A sequence of operations, including mosaic, clipping, and reprojection, were applied to the original GLC_FCS30 dataset in order to acquire the spatial distribution of forests in China. The land-cover data were resampled to 1-km spatial resolution using the nearest neighbor method to ensure consistency with the LAI datasets [Moderate Resolution Imaging Spectroradiometer (MODIS) and Global Land Surface Satellite (GLASS)] and to facilitate intercomparisons at the 1-km spatial resolution.

D. LAI Products

The MODIS and GLASS LAI products were selected to compare with our results from ICESat-2 in forest areas in China. The MODIS Collection 6 LAI products (MOD15A2H) spanning from 2019 to 2020 were sourced from the Google Earth Engine Cloud Platform (https://earthengine.google.com), which had a spatial resolution of 500 m and a temporal resolution of 8 days. The GLASS LAI product [53] between 2019 and 2020 was downloaded from the National Earth System Science Data Center, China (https://www.geodata.cn), which had an 8-day interval and a spatial resolution of 500 m. The MODIS LAI and GLASS LAI were processed through a routine of mosaicking, resampling, reprojecting, and compositing to acquire the data at 1-km spatial and 1-month temporal resolution. This processed LAI dataset was then employed for comparison with ICESat-2 LAI.

III. Methods

A QC method was proposed to screen out the good-quality photon distribution from ICESat-2 100-m segments, which

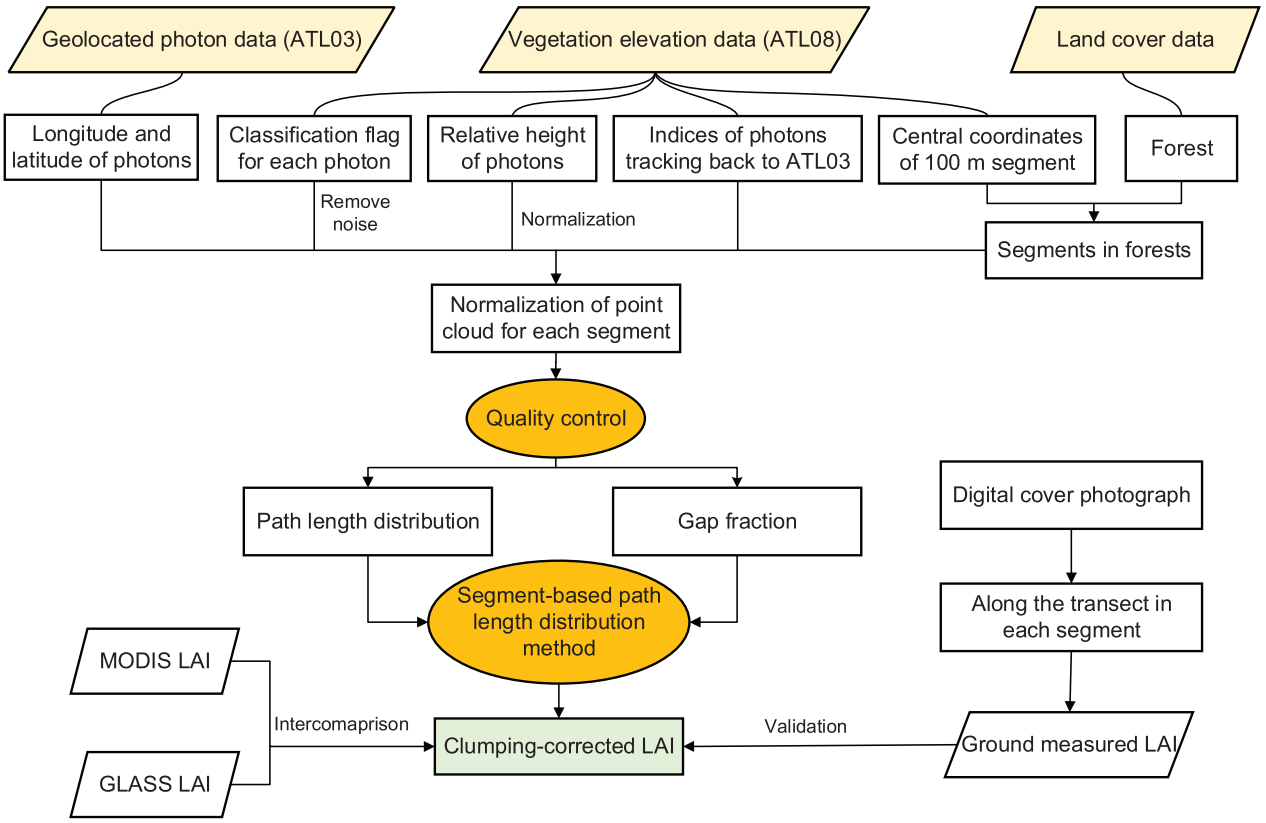

Fig. 2. Flowchart of forest LAI retrieval using ICESat-2 data.

employed the number of 10-m windows without ground points in the ICESat-2 100-m segment as the QC flag. Then, the segment-based path length distribution method was used to correct the clumping effect and retrieve the actual LAI. Finally, the LAI with various QC flags was compared with the field measurements to assess the performance of the QC method. The workflow of LAI retrieval with QC flags is provided in Fig. 2.

A. QC Method for LAI Retrieval Based on ICESat-2 Segments

The ICESat-2 segments with good-quality photon distribution [see Fig. 3(a)] play an important role in determining the reliability of LAI inversion [43]. The ICESat-2 raw data inherently incorporate ambient noises stemming from the concurrent capture of solar background photons and genuine signal photons by the ATLAS sensor [44]. Although the ATL08 product was generated by denoise and height normalization from ATL03, the distribution of point cloud in the ATL08 100-m segment may include issues of missing point cloud [see Fig. 3(b) and (c)] and incomplete height normalization [see Fig. 3(d) and (e)], which is not suitable to invert LAI and causes large uncertainty. Guo et al. [43] founded that the good quality of point cloud improves the accuracy of LAI retrieval. Thus, we proposed a QC method for efficiently screening high-quality point cloud data in segments in order to improve the accuracy of large-scale LAI inversion by ICESat-2 data. We assumed that the ICESat-2 laser beam could penetrate the forest canopy in our study area, meaning that there should be some ground points even when the canopy is dense. The proposed method for QC of ICESat-2 data includes three steps:

1) Divide the ATL08 100-m segment into ten 10-m windows.
2) Count the number of ground points in each 10-m window. The height threshold of 2 m was used to distinguish the canopy and ground points.
3) Record the number of 10-m windows without ground points in the 100-m segment, which was used as the QC flag of the 100-m segment.

The definition of the QC flag for 100-m segments based on our method is shown in Table I, while Fig. 4 illustrates examples of segments with varying QC levels. The QC flag of the 100-m segment was 0 when the 100-m segment had no 10-m window

TABLE I
DEFINITION OF THE QC FLAG OF ICESAT-2 100-M SEGMENTS

Quality control	The number of 10 m windows without ground points
0	0
1	1
2	2
⋮	⋮
9	9
10	10

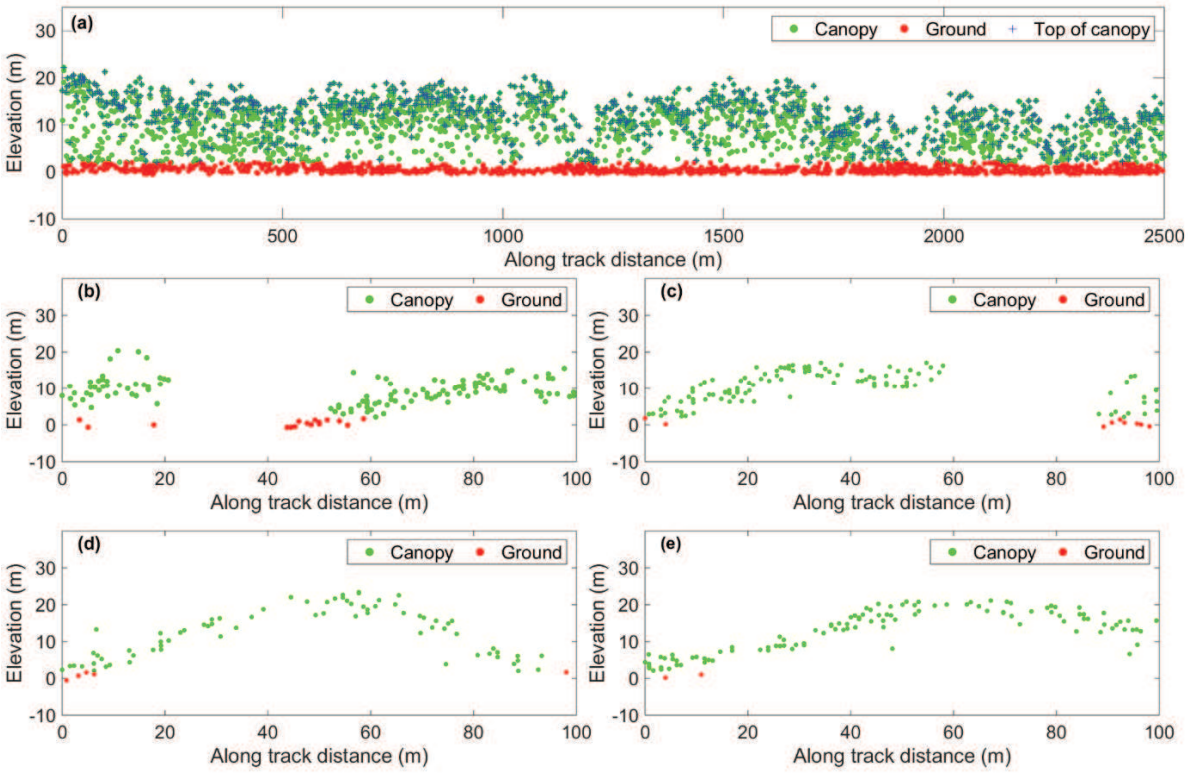

Fig. 3. Distribution of point clouds in the ATL08 segment. (a) Good-quality point cloud, (b) and (c) point cloud missing, and (d) and (e) incomplete height normalization.

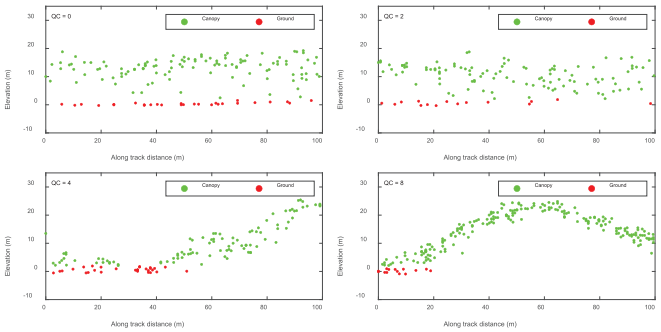

Fig. 4. Different QC levels of 100-m segment.

without ground points. If only one 10-m window lacked a ground point, the flag of QC was 1; if two 10-m windows had no ground points, the flag of QC was 2, and so on. In general, the ATL08 100-m segments were divided into 11 QC levels (from 0 to 10) based on our method, and the high value of the QC flag meant that the inversion of LAI in the 100-m segment was less reliable. Specifically, we removed the 100-m segments that had a QC flag of 10 because there were no ground points in the segment.

B. Clumping-Corrected LAI Retrieval

The clumping-corrected LAI was retrieved from ICESat-2 data using the segment-based path length distribution method [43]. The segment is defined as along-track span of the photon from a single ground track. In this study, the 100-m segment of ATL08 was used to extract gap fraction and path length distribution for clumping-corrected LAI retrieval by the segment-based path length distribution method. The gap fraction (P) can be derived from LiDAR metrics, which can be calculated as the number-based ratio method [46]

$$P = N_{\text{ground}} \big/ N_{\text{all}} \tag{1}$$

where N_{ground} represents the number of ground points and N_{all} denotes the total number of points in the segment. The 2-m height threshold was used to distinguish between canopy and ground photons.

The path length distribution can be acquired from the statistics of the top of canopy, and the top of canopy was obtained by searching the maximum height using a 1-m moving window in the 100-m segment. The path length distribution $[p_{lr}(lr)]$ within the segment is defined as follows:

$$p_{lr}(lr) = \frac{\hat{p}_{lr}(lr)}{\int_0^1 \hat{p}_{lr}(lr)d(lr)} \tag{2}$$

$$lr = l/l_{\max} \tag{3}$$

where lr is the relative path length normalized to [0, 1], l is the absolute path length at a location of a transect, and $l_{\max}$ is the maximum path length along the transect. $\hat{p}_{lr}(lr)$ is the frequency of lr falling within the infinitesimal interval $[lr, lr + d(lr)]$.

The path length distribution and gap fraction of the 100-m segment were input to the path length distribution model [7],

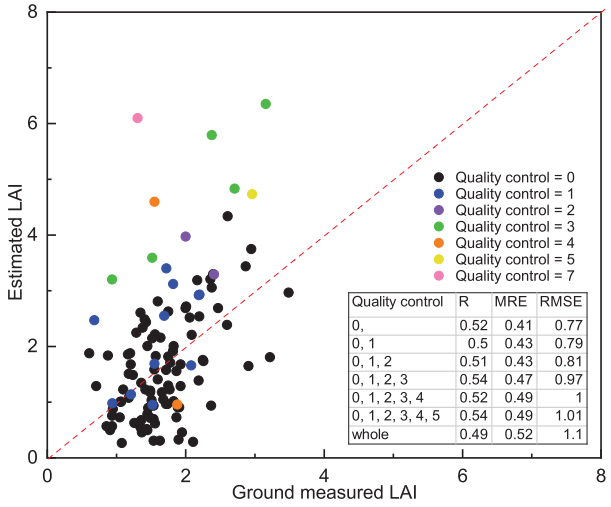

Fig. 5. Scatterplot showing the relationship between ground-measured LAI and LAI retrievals for segments with different levels of QC. The dashed line represents a 1:1 line.

[42] to model the clumping effect and retrieve the actual LAI

$$\mathrm{LAI} = \int_0^1 (\mathrm{FAVD} \cdot l_{\max}) \cdot lr \cdot p_{lr}(lr) d(lr) \tag{4}$$

where FAVD is the leaf area volume density. The intermediate variables $\mathrm{FAVD} \cdot l_{\max}$ can be derived by solving

$$P = \int_0^1 e^{-G \cdot (\mathrm{FAVD} \cdot l_{\max}) \cdot lr} \cdot p_{lr}(lr) d(lr) \tag{5}$$

where P is the gap fraction, G is the leaf projection coefficient, and it is set as 0.5 for canopies with a spherical distribution of leaf angles.

The clumping index (CI) was calculated according to [54]

$$\mathrm{CI} = \mathrm{LAI_e}/\mathrm{LAI} \tag{6}$$

where $\mathrm{LAI_e}$ is the effective LAI, which can be calculated by Beer's law.

Although the segment-based path length distribution method has successfully been used to derive LAI using ICESat-2 data on a regional scale, it has not been tested for the inversion of LAI on a large scale. Therefore, we integrated ATL03 and ATL08 products to acquire the photon data with relative height and positional information as the input data for this method to estimate clumping-corrected LAI on a large scale for forested sites in China (see Fig. 2). The ground-measured LAI from the digital cover photograph, whose location was identical to ICESat-2 ground tracks, was used to validate the LAI retrievals.

IV. Results

A. Comparison of ICESat-2-Derived LAI With Ground Measurements

The ICESat-2 LAI for the 100 × 11 m segments was derived from the path length distribution and assigned a QC level using our proposed QC method. The ICESat-2 LAI was compared with field-measured LAI to evaluate the effectiveness of the QC method in improving the accuracy of ICESat-2 LAI (Fig. 5). In the whole, the results showed a good agreement between ICESat-2 LAI and ground-measured LAI, with a Pearson correlation coefficient (R) of 0.49, a mean relative error (MRE) of 0.52, and a root mean square error (RMSE) of 1.10. Moreover, we analyzed the accuracy of ICESat-2 LAI with different QC flags based on ground measurements. The results showed that ICESat-2 LAI with a QC flag of 0 performed better than other LAIs with a QC flag over 0, with an RMSE of 0.77.

In addition, we found that the ICESat-2 LAI with the QC flags of 0, 1, and 2 also performed well, and the error indicators (R, MRE, and RMSE) were not significantly different between the ICESat-2 with the QC flag of 0. The RMSE of the LAI derived from the ICESat-2 good-quality (QC < 3) segments decreased 26.36% relative to the LAI derived from all segments, which indicated that the LAIs of QC flags less than 3 (good-quality segments) were more reliable than others.

TABLE II

Error Indicators of ICESat-2 LAI With MODIS LAI and GLASS LAI Based on Different QC Flags. QC < 1 Means the Values of QC Flags of 100-m Segments Were Less Than 1 (QC = 0)

	ICESat-2 vs MODIS			ICESat-2 vs GLASS		
QC	R	MRE	RMSE	R	MRE	RMSE
QC < 1	0.55	1.01	1.10	0.59	0.60	1.37
QC < 2	0.52	1.14	1.20	0.56	0.66	1.40
QC < 3	0.48	1.30	1.34	0.54	0.72	1.43
QC < 4	0.46	1.45	1.53	0.52	0.78	1.49
QC < 5	0.43	1.61	1.74	0.51	0.84	1.57
QC < 6	0.41	1.75	1.93	0.49	0.90	1.67
QC < 7	0.40	1.86	2.06	0.48	0.95	1.75
QC < 8	0.38	1.93	2.14	0.47	0.98	1.81
QC < 9	0.38	1.95	2.17	0.46	0.99	1.83
QC < 10	0.37	1.96	2.18	0.46	1.00	1.84

Notes: progressive blue represents better performance, and progressive red represents worse performance.

B. Comparison of ICESat-2 LAI, MODIS LAI, and GLASS LAI Based on Different QC Flags

We aggregated 100-m segments of ICESat-2 data to 1-km pixel of MODIS and GLASS data for comparison and assessing the performance of the QC method in improving the accuracy of ICESat-2 LAI. Specifically, the monthly averaged values of ICESat-2 LAI, MODIS LAI, and GLASS LAI were used to intercomparison, with the exclusion of cases that there are less than five 100-m segments within a 1-km pixel. The results showed that ICESat-2 segments with QC < 1 (QC = 0) performed better than segments with other QC, which had the highest correlation coefficient and lowest MRE and RMSE (see Table II). Moreover, the ICESat-2 LAI with QC < 3 (QC = 0, 1, and 2) also had a good agreement with MODIS LAI and GLASS LAI, respectively, and the error indicators (R, MRE, and RMSE) were not significantly different from the ICESat-2 LAI with QC = 0, which indicated that the LAIs with QC < 3 had an acceptable accuracy. In addition, we also compared

TABLE III

RMSE BETWEEN ICESAT-2 LAI WITH MODIS LAI AND GLASS LAI ACROSS FOREST TYPES BASED ON DIFFERENT QC FLAGS. QC < 1 MEANS THE VALUES OF QC FLAGS OF 100-M SEGMENTS WERE LESS THAN 1 (QC = 0)

	ICESat-2 vs MODIS					ICESat-2 vs GLASS				
	EBF	DBF	ENF	DNF	MF	EBF	DBF	ENF	DNF	MF
QC < 1	1.56	1.14	1.09	1.02	0.88	1.99	1.50	1.15	1.17	0.88
QC < 2	1.49	1.19	1.35	1.10	1.14	1.82	1.50	1.27	1.20	1.01
QC < 3	1.52	1.27	1.64	1.22	1.38	1.62	1.49	1.43	1.24	1.09
QC < 4	1.68	1.41	1.93	1.36	1.65	1.47	1.50	1.62	1.33	1.22
QC < 5	1.91	1.58	2.20	1.52	1.89	1.40	1.55	1.81	1.44	1.34
QC < 6	2.12	1.74	2.42	1.66	2.09	1.42	1.63	1.98	1.56	1.49
QC < 7	2.25	1.87	2.56	1.76	2.19	1.47	1.70	2.09	1.64	1.58
QC < 8	2.33	1.95	2.65	1.82	2.24	1.50	1.76	2.17	1.69	1.63
QC < 9	2.36	1.98	2.68	1.84	2.27	1.52	1.78	2.20	1.72	1.65
QC < 10	2.36	1.99	2.69	1.85	2.27	1.52	1.79	2.20	1.72	1.66

Notes: evergreen broadleaved forest (EBF), deciduous broadleaved forest (DBF), evergreen needle-leaved forest (ENF), deciduous needle-leaved forest (DNF), and mixed forest (MF). Progressive green represents better performance, and progressive red represents worse performance.

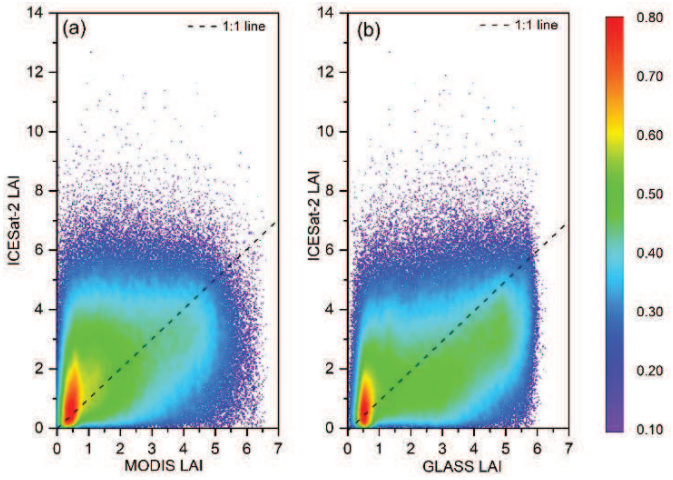

Fig. 6. Comparison of ICESat-2 LAI with (a) MODIS LAI and (b) GLASS LAI in forest areas in China.

the ICESat-2 LAI with QC of 0, 1, and 2 with MODIS LAI and GLASS LAI in order to explore whether ICESat-2 LAI avoided the saturation phenomenon that happened to passive optical data. The results (see Fig. 6) showed that ICESat-2 LAI had a larger LAI range than MODIS LAI and GLASS LAI, and MODIS LAI and GLASS LAI showed saturation when LAI over 6.5 and 6.0, respectively.

The comparison of ICESat-2 LAI with MODIS LAI and GLASS LAI across forest types also showed that the segments with a good quality of point cloud acquire relatively reliable LAI retrieval. The statistics of RMSE (see Table III) showed that ICESat-2 LAI with QC < 1 (QC = 0) had the best performance (lowest RMSE) in DBFs, evergreen needle-leaved forests, DNFs, and MFs, while it is an obvious difference in EBFs. Moreover, we found that the ICESat-2 LAI with QC < 3 (QC = 0, 1, and 2) also had a good agreement with MODIS LAI and GLASS LAI across all forest types, and there was no significant difference in RMSE between ICESat-2 LAI with QC < 3 and QC < 1. In general, the LAIs derived from ICESat-2 segments with QC flags of 0–2 were relatively reliable in all forest types, which can be used to analyze the spatial distribution of ICESat-2 LAI in forest areas in China.

C. Comparison of ICESat-2 LAI, MODIS LAI, and GLASS LAI Based on Different Forest Growth Stages

We conducted a comparison of ICESat-2 LAI with QC of 0–2 with MODIS LAI and GLASS LAI across the three growth stages: the beginning of growing season (from April to May), the middle of growing season (from June to August), and the end of growing season (from September to October). We divided LAI values into four ranges, including 0–2, 2–4, 4–6 and over 6 for comparison. The percentage of LAI values ranging from 2 to 4, 4 to 6, and over 6 from three datasets was the highest in the middle of growing season, followed by the end of growing season, and the lowest in the beginning of growing season (see Fig. 7). In the beginning of growing season [see Fig. 7(a)], GLASS LAI had no values greater than 6, and the proportion of ICESat-2 and MODIS LAI values greater than 6 accounted for 0.94% and 0.10%, respectively. The ratio of MODIS LAI below 2 was the highest, accounting for about 86% of the total values, and ICESat-2 LAI had the least proportion of LAI below 2. In the middle of growing season [see Fig. 7(b)], the amount of LAI values over 6 was the most from ICESat-2 (1.34%), followed by MODIS (0.24%) and GLASS (0.05%). The proportion of GLASS LAI values ranged from 4 to 6 was most (45%), followed by MODIS (19%) and ICESat-2 (15%). The GLASS LAI values less than 2 were the least (9.43%), and ICESat-2 and MODIS LAI had approximately 37% and 33% values less than 2, respectively. In the end of the growing season [see Fig. 7(c)], the proportion of ICESat-2 LAI values over 6 was the highest (0.60%), followed by MODIS (0.18%); the lowest was GLASS (0.02%). The proportions of ICESat-2, MODIS and GLASS LAI values ranging from 4 to 6 were 7%, 1.8%, and 2.5%, respectively.

Significantly, the MODIS LAI and GLASS LAI values within 4–6 exhibited a decline of approximately 17% and 43%, respectively, from the middle to the end of the growing season because leaves of deciduous forests changed from green to

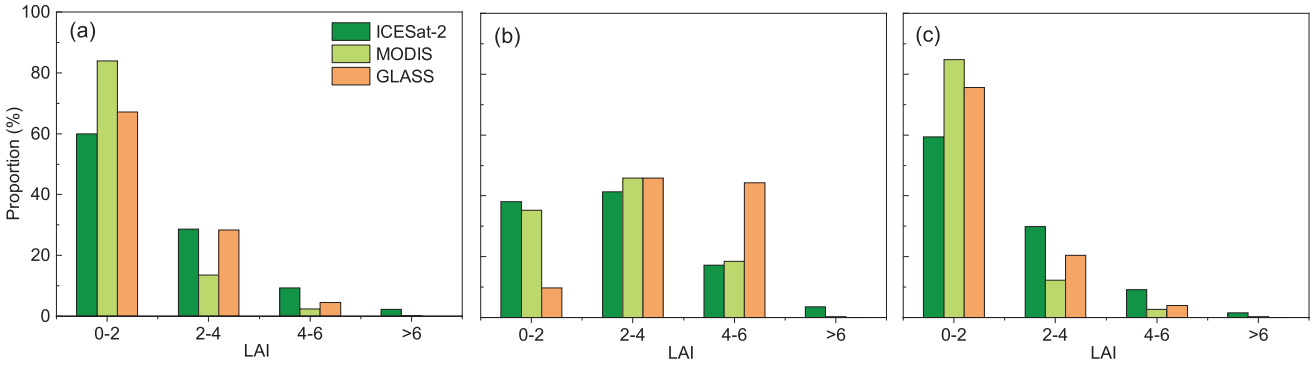

Fig. 7. Comparison of ICESat-2 LAI, MODIS LAI, and GLASS LAI in different growth stages from (a) April to May, (b) June to August, and (c) September to October.

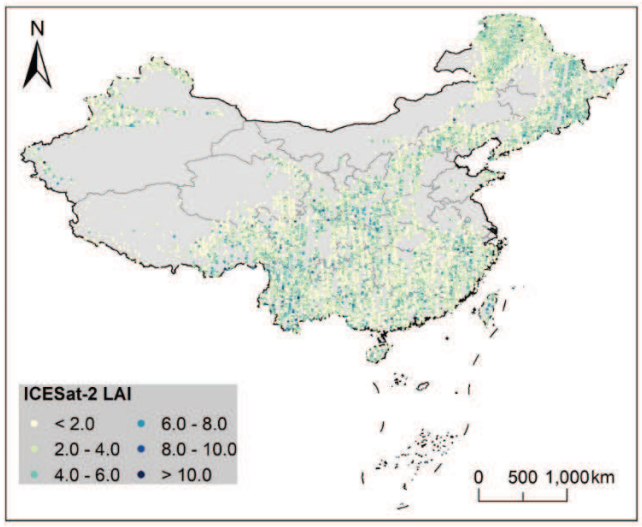

Fig. 8. Spatial distribution of ICESat-2 LAI in Chinese forest areas from June to August 2019. The dots represent the ICESat-2 100-m segment.

yellow, causing spectrum changes. In the middle of growing season, the DBF accounted for 64.3% and 62.7% of the LAI values ranging from 4 to 6 for MODIS LAI and GLASS LAI, respectively (see Table S1). The DNF accounted for 17.8% and 15.3% of the LAI values, ranging from 4 to 6 for MODIS LAI and GLASS LAI, respectively. At the end of the growing season, the contribution of DBF to the LAI values within 4–6 decreased to 23% and 8% for MODIS LAI and GLASS LAI, respectively (see Table S2). The DNF accounted for 0.2% and 0% of the LAI values ranging from 4 to 6 for MODIS LAI and GLASS LAI, respectively. In contrast, ICESat-2 LAI values from both DBFs and DNFs showed only 2% changes from the middle to the end of the growing season because ICESat-2 was insensitive to spectral changes.

D. Characteristics of ICESat-2 LAI in the Forested Ecozone

LAI estimates were derived using the segment-based path length distribution method to on-orbit ICESat-2 data. The estimates were obtained for the entire Chinese forest biome in 100 × 11 m segments from April to October 2019 and 2020, and Fig. 8 shows the spatial distribution of ICESat-2 LAI in forest areas in China from June to August 2019. The retrieval process encompassed approximately 2.5 million segments during the study period.

Overall, the distribution of ICESat-2 LAI [see Fig. 9(a)] across forest areas in China was largely skewed toward lower LAI values. More than 55% of the segments exhibited LAI values below 2.0, and the median and mean LAI values in forested areas were 1.72 and 2.11, respectively. The ICESat-2 LAI gathered by forest types [see Fig. 9(b)] showed that ICESat-2 LAI had considerable variability within forested ecozones during the period of 2019 and 2020. The average LAI ranged from 1.93 in DNFs to 2.59 in MFs. DBFs accounted for the greatest proportion of ICESat-2 segments, accounting for approximately 50% of the total segments. EBF and MF comprised the low proportion of ICESat-2 segments, with percentages of 9% and 1%, respectively. The MF exhibited the highest median LAI value at 2.30, and DNFs presented the lowest median LAI value (1.54), followed by ENFs (1.90). Notably, EBFs had relatively dense canopies, and the segments with LAI greater than 6.0 accounted for 4.05%, followed by MF (3.75%). DNFs displayed relatively sparse canopies, with a significant proportion (59.12%) of segments having LAI values below 2.0. In addition, CI across forest area was mainly concentrated in the range of 0.7–0.9, accounting for about 69% of the total segments [see Fig. 9(c)]. The CI was different in various forest types. The average CI ranged from 0.75 in MFs to 0.81 in ENF [see Fig. 9(d)].

V. Discussion

A. ICESat-2 LAI Dynamics in Different Stages of Growing Season

The comparison of ICESat-2 LAI with MODIS LAI and GLASS LAI was conducted to evaluate the performance of ICESat-2 LAI in different stages of growing season. We found that the proportions of LAI over 2.0 from ICESat-2, MODIS, and GLASS were the highest in the middle of growing season, followed by the end of growing season, and the lowest in the beginning of growing season (see Fig. 7). In different stages of growing season, the proportion of LAI over 6.0 from ICESat-2 was highest among three LAI datasets, and MODIS LAI and GLASS LAI exhibited a tendency to saturate as LAI surpassed 6.5 and 6.0, respectively. This divergence

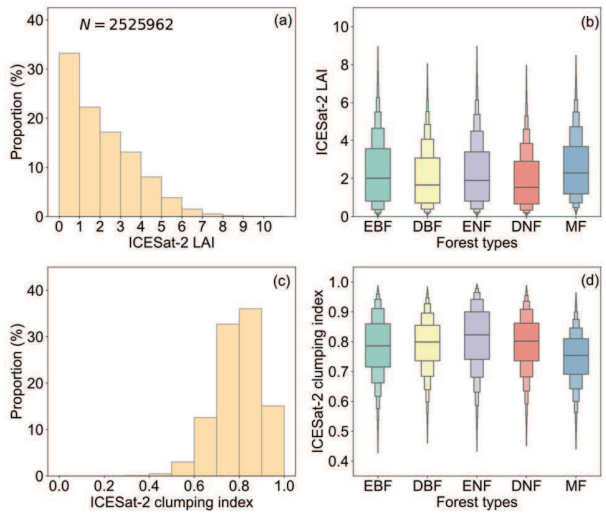

Fig. 9. Distributions of ICESat-2 LAI and CI across forest areas in China and different forest ecozones EBF, DBF, ENF, DNF, and MF: (a) histogram of LAI for all forests; (b) LAI by forest type; (c) histogram of CI for all forests; and (d) CI by forest type.

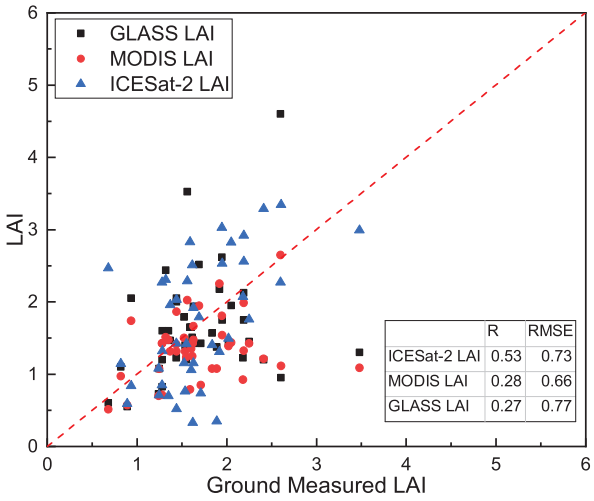

Fig. 10. Comparison of ground observations with ICESat-2 LAI, MODIS LAI, and GLASS LAI.

can primarily be attributed to the limited penetrability of passive optical remote sensing data (MODIS and GLASS) in dense forest canopies, leading to signal saturation [55]. ICESat-2 is active LiDAR with the capability to penetrate dense canopies and capture intricate internal canopy information, thus effectively mitigating the saturation phenomenon [56], [57]. In addition, our results had a subtle difference Zhang et al. [55] about when MODIS LAI is saturated, a discrepancy that might arise from differing study areas. While their results focused on LAI retrieval within a regional scope, our study encompassed nationwide LAI estimation across China.

Moreover, the significant decline of 17% and 43% in LAI ranging from 4.0 to 6.0 from MODIS LAI and GLASS LAI was found from the middle to end of growing season [see Fig. 7(b) and (c)], which may be related to the sensitivity of passive optical data to spectral changes caused by the variation of chlorophyll in leaves [58]. The yellowing process of leaves may be the main factor causing this apparent decline, which usually happens in deciduous forests. In order to verify this conjecture, we conducted a statistical analysis of three LAI datasets according to different LAI ranges and growth stages (see Tables S1 and S2). We found that the MODIS LAI and GLASS LAI ranging from 4.0 to 6.0 had a decline of approximately 42% and 55% in DBFs from the middle to end of growing season and 18% and 15% in DNFs. In contrast, the ICESat-2 LAI ranging from 4.0 to 6.0 only decreased about 2% from the middle to the end of growing season for DBFs and DNFs, respectively, which indicated that ICESat-2 LAI was insensitive to the pigment shifts in leaves.

B. Performance of ICESat-2 LAI at Pixel Scale

ICESat-2 LAI showed a good performance at segment scale according to our results, but the feasibility of generating gridded LAI at pixel scale is still unclear. The comparison of ground measurements with ICESat-2 LAI, MODIS LAI, and GLASS LAI was conducted at a pixel resolution of 1 km to evaluate the potential of gridded LAI generation by ICESat-2. Specifically, ICESat-2 LAIs with QC flags of 0–2 were selected for this comparison. We found that ICESat-2 LAI had a satisfactory performance (see Fig. 10), and the scatter points corresponding to ICESat-2 LAI clustered closely around the 1:1 reference line, whereas MODIS LAI and GLASS LAI displayed some marked deviations, particularly when LAI surpassed 2.5. Moreover, ICESat-2 LAI had a stronger correlation with ground-measured LAI than MODIS LAI and GLASS LAI, with a correlation coefficient of 0.53. However, MODIS LAI had the lowest RMSE (0.66), followed by ICESat-2 LAI (0.73), and the highest RMSE was GLASS LAI (0.77). The reason may be that there are few segments (like one or two) within a 1-km pixel, and this is insufficient spatial representation. Moreover, the ground measurements were primarily used to validate the LAI within a 100-m segment, and it is unsuitable for comprehensive validation at the 1-km pixel scale. Therefore, future studies should focus on the spatial representativeness of ground sampling and try to select as many 100-m segments as possible within the 1-km pixel scale.

C. Limitations and Opportunities

ICESat-2 employs a unique photon counting sampling method, which provides a potential possibility for clumping-corrected LAI retrieval at a large scale [59], but the accuracy of LAI retrieval still depends on the quality of normalized point cloud data. The proposed QC method in this study provides the possibility of quickly screening out high-quality point cloud data, and combining it with the segment-based path length distribution method could efficiently invert clumping-corrected LAI at a large scale. Notably, the segment-based path length distribution method relies solely on the 3-D structural information from the LiDAR point cloud for LAI retrieval, with no direct computation using land-cover data or reliance on additional parameters, resulting in good methodological universality. However, we use land-cover data to filter

ICESat-2 segments, retaining only forest-classified regions for LAI calculation. Land-cover misclassification may introduce uncertainties in two scenarios: 1) actual forest areas mislabeled as nonforest will be excluded, leading to data gaps but no direct bias in LAI estimates and 2) nonforest areas misclassified as forest may yield unreliable LAI values. For example, grasslands incorrectly labeled as forest typically exhibit point cloud returns below 2 m in height, resulting in a gap fraction near 1 and an LAI estimate approaching 0 due to ICESat-2's limited sensitivity to low vegetation. Conversely, nonvegetated surfaces (e.g., buildings) misclassified as forest may produce spurious LAI values if tall (>2 m) structures are present, despite their true LAI being 0. While forest structural distinctiveness generally ensures reliable identification in land-cover products, ensuring spatiotemporal consistency between ICESat-2 data and land-cover maps can mitigate errors from land-cover changes or misregistration.

Nonetheless, LAI retrieval from spaceborne LiDAR is still distributed along the flight trajectory, which severely limits the study of spatiotemporal changes in forest structure. Many studies conducted the fusion of ICESat-2 data and passive optical imagery to map spatially continuous canopy height and biomass at regional scale [38], [60], [61], [62], [63], which also provide a reference for exploring the combination of ICESat-2 data with wall-to-wall imagery (passive optical or microwave) to generate spatially continuous LAI.

VI. Conclusion

As ICESat-2 continues to sample forested ecozones, the synoptic measurements of ICESat-2 will provide more dense spatial coverage of canopy height and create an incredible opportunity to enhance estimates of forest LAI on large scales. This study proposed a QC method by the number of 10-m windows without ground points in the ICESat-2 100-m segment as the QC flag to improve the accuracy of LAI retrieval by ICESat-2 data. Our results showed that the proposed method is feasible to improve the accuracy of ICESat-2 LAI, and the LAI derived from the ICESat-2 good-quality (QC < 3) segments had good accuracy, whose RMSE decreased 26.36% relative to all ICESat-2 LAIs. Moreover, ICESat-2 LAI with QC < 3 was reliable because it had good agreement with ground measurements, MODIS LAI and GLASS LAI. ICESat-2 LAI mitigated the saturation problem of passive optical remote sensing when LAI was over 6.0. In general, our proposed method efficiently improves the accuracy of LAI derived from ICESat-2, and its application in forest areas in China highlights its effectiveness in improving the accuracy of ICESat-2 LAI at a large scale.

VII. Acknowledgment

The authors would like to thank the National Snow and Ice Data Center, Boulder, CO, USA, for providing the Ice, Cloud, and land Elevation Satellite-2 (ICESat-2) data, CASEarth for providing the land-cover data, and Global Land Surface Satellite (GLASS) and Moderate Resolution Imaging Spectroradiometer (MODIS) Science Team for providing the leaf area index (LAI) products.

References

[1] H. H. Shugart, S. Saatchi, and F. G. Hall, "Importance of structure and its measurement in quantifying function of forest ecosystems," *J. Geophys. Res., Biogeosci.*, vol. 115, no. G00E13, Jun. 2010, doi: 10.1029/2009JG000993.

[2] P. Ciais et al., "Carbon accumulation in European forests," *Nature Geosci.*, vol. 1, no. 7, pp. 425–429, 2008.

[3] Y. Li et al., "Biophysical impacts of Earth greening can substantially mitigate regional Land Surface Temperature warming," *Nature Commun.*, vol. 14, no. 1, pp. 121–133, Jan. 2023.

[4] A. Swatantran, R. Dubayah, D. Roberts, M. Hofton, and J. B. Blair, "Mapping biomass and stress in the Sierra Nevada using LiDAR and hyperspectral data fusion," *Remote Sens. Environ.*, vol. 115, no. 11, pp. 2917–2930, Nov. 2011.

[5] G. Simioni, G. Marie, and R. Huc, "Influence of vegetation spatial structure on growth and water fluxes of a mixed forest: Results from the NOTG 3D model," *Ecolog. Model.*, vol. 328, pp. 119–135, May 2016.

[6] J. M. Chen, P. M. Rich, S. T. Gower, J. M. Norman, and S. Plummer, "Leaf area index of boreal forests: Theory, techniques, and measurements," *J. Geophys. Res., Atmos.*, vol. 102, no. D24, pp. 29429–29443, Dec. 1997.

[7] G. Yan et al., "Review of indirect optical measurements of leaf area index: Recent advances, challenges, and perspectives," *Agricult. Forest Meteorol.*, vol. 265, pp. 390–411, Feb. 2019.

[8] M. A. Wulder et al., "LiDAR sampling for large-area forest characterization: A review," *Remote Sens. Environ.*, vol. 121, pp. 196–209, Jun. 2012.

[9] S. S. Saatchi et al., "Benchmark map of forest carbon stocks in tropical regions across three continents," *Proc. Nat. Acad. Sci. USA*, vol. 108, no. 24, pp. 9899–9904, Jun. 2011.

[10] W. Fan, Y. Gai, X. Xu, and B. Yan, "The spatial scaling effect of the discrete-canopy effective leaf area index retrieved by remote sensing," *Sci. China Earth Sci.*, vol. 56, no. 9, pp. 1548–1554, Sep. 2013.

[11] F. Baret et al., "LAI, fAPAR and fCover CYCLOPES global products derived from VEGETATION," *Remote Sens. Environ.*, vol. 110, no. 3, pp. 275–286, Oct. 2007.

[12] R. Myneni, Y. Knyazikhin, and T. Park, *MOD15A2H MODIS Leaf Area Index/FPAR 8-Day L4 Global 500m SIN Grid V006*. Washington, DC, USA: NASA EOSDIS Land Processes DAAC, 2015.

[13] Z. Xiao et al., "Use of general regression neural networks for generating the GLASS leaf area index product from time-series MODIS surface reflectance," *IEEE Trans. Geosci. Remote Sens.*, vol. 52, no. 1, pp. 209–223, Jan. 2014.

[14] Z. Zhu et al., "Global data sets of vegetation leaf area index (LAI)3G and fraction of photosynthetically active radiation (FPAR)3g derived from global inventory modeling and mapping studies (GIMMS) normalized difference vegetation index (NDVI3G) for the period 1981 to 2011," *Remote Sens.*, vol. 5, no. 2, pp. 927–948, Feb. 2013.

[15] S. Piao et al., "Detection and attribution of vegetation greening trend in China over the last 30 years," *Global Change Biol.*, vol. 21, no. 4, pp. 1601–1609, Apr. 2015.

[16] Z. Zhu et al., "Greening of the Earth and its drivers," *Nature Climate Change*, vol. 6, no. 8, pp. 791–795, 2016.

[17] Z. Zhu, S. Piao, and X. Lian, "Attribution of seasonal leaf area index trends in the northern latitudes with 'optimally' integrated ecosystem models," *Global Change Biol.*, vol. 23, no. 11, pp. 4798–4813, 2017.

[18] C. Chen et al., "China and India lead in greening of the world through land-use management," *Nature Sustainability*, vol. 2, no. 2, pp. 122–129, Feb. 2019.

[19] J. M. Chen et al., "Vegetation structural change since 1981 significantly enhanced the terrestrial carbon sink," *Nature Commun.*, vol. 10, no. 1, p. 4259, Sep. 2019.

[20] H. Tang et al., "Retrieval of vertical LAI profiles over tropical rain forests using waveform LiDAR at La Selva, Costa Rica," *Remote Sens. Environ.*, vol. 124, pp. 242–250, Sep. 2012.

[21] X. Yang, C. Wang, F. Pan, S. Nie, X. Xi, and S. Luo, "Retrieving leaf area index in discontinuous forest using ICESat/GLAS full-waveform data based on gap fraction model," *ISPRS J. Photogramm. Remote Sens.*, vol. 148, pp. 54–62, Feb. 2019.

[22] X. Zhu, S. Nie, C. Wang, X. Xi, J. Lao, and D. Li, "Consistency analysis of forest height retrievals between GEDI and ICESat-2," *Remote Sens. Environ.*, vol. 281, Nov. 2022, Art. no. 113244.

[23] L. Tian, Y. Qu, and J. Qi, "Estimation of forest LAI using discrete airborne LiDAR: A review," *Remote Sens.*, vol. 13, no. 12, p. 2408, Jun. 2021.

[24] S. Luo, C. Wang, G. Li, and X. Xi, "Retrieving leaf area index using ICESat/GLAS full-waveform data," *Remote Sens. Lett.*, vol. 4, no. 8, pp. 745–753, Aug. 2013.
[25] H. Tang, R. Dubayah, M. Brolly, S. Ganguly, and G. Zhang, "Large-scale retrieval of leaf area index and vertical foliage profile from the spaceborne waveform LiDAR (GLAS/ICESat)," *Remote Sens. Environ.*, vol. 154, pp. 8–18, Nov. 2014.
[26] H. Tang, S. Ganguly, G. Zhang, M. A. Hofton, R. F. Nelson, and R. Dubayah, "Characterizing leaf area index (LAI) and vertical foliage profile (VFP) over the United States," *Biogeosciences*, vol. 13, no. 1, pp. 239–252, Jan. 2016.
[27] J. Tian, L. Wang, X. Li, C. Shi, and H. Gong, "Differentiating tree and shrub LAI in a mixed forest with ICESat/GLAS spaceborne LiDAR," *IEEE J. Sel. Topics Appl. Earth Observ. Remote Sens.*, vol. 10, no. 1, pp. 87–94, Jan. 2017.
[28] L. Cui et al., "Retrieval of vertical foliage profile and leaf area index using transmitted energy information derived from ICESat GLAS data," *Remote Sens.*, vol. 12, no. 15, p. 2457, Jul. 2020.
[29] K. Rishmawi, C. Huang, and X. Zhan, "Monitoring key forest structure attributes across the conterminous United States by integrating GEDI LiDAR measurements and VIIRS data," *Remote Sens.*, vol. 13, no. 3, p. 442, Jan. 2021.
[30] H. Jiang et al., "Clumping effects in leaf area index retrieval from large-footprint full-waveform LiDAR," *IEEE Trans. Geosci. Remote Sens.*, vol. 60, 2022, Art. no. 4406220.
[31] R. V. Leite et al., "Large scale multi-layer fuel load characterization in tropical savanna using GEDI spaceborne LiDAR data," *Remote Sens. Environ.*, vol. 268, Jan. 2022, Art. no. 112764.
[32] Y. Wang et al., "Retrieval and validation of vertical LAI profile derived from airborne and spaceborne LiDAR data at a deciduous needleleaf forest site," *GISci. Remote Sens.*, vol. 60, no. 1, Dec. 2023, Art. no. 2214987.
[33] A. L. Neuenschwander, T. J. Urban, R. Gutierrez, and B. E. Schutz, "Characterization of ICESat/GLAS waveforms over terrestrial ecosystems: Implications for vegetation mapping," *J. Geophys. Res., Biogeosci.*, vol. 113, no. G02S03, Jun. 2008, doi: 10.1029/2007JG000557.
[34] M. Queinnec, J. C. White, and N. C. Coops, "Comparing airborne and spaceborne photon-counting LiDAR canopy structural estimates across different boreal forest types," *Remote Sens. Environ.*, vol. 262, Sep. 2021, Art. no. 112510.
[35] X. Liu et al., "Neural network guided interpolation for mapping canopy height of China's forests by integrating GEDI and ICESat-2 data," *Remote Sens. Environ.*, vol. 269, Feb. 2022, Art. no. 112844.
[36] C. Mulverhill, N. C. Coops, T. Hermosilla, J. C. White, and M. A. Wulder, "Evaluating ICESat-2 for monitoring, modeling, and update of large area forest canopy height products," *Remote Sens. Environ.*, vol. 271, Mar. 2022, Art. no. 112919.
[37] L. L. Narine, S. Popescu, A. Neuenschwander, T. Zhou, S. Srinivasan, and K. Harbeck, "Estimating aboveground biomass and forest canopy cover with simulated ICESat-2 data," *Remote Sens. Environ.*, vol. 224, pp. 1–11, Apr. 2019.
[38] S. Nandy, R. Srinet, and H. Padalia, "Mapping forest height and aboveground biomass by integrating ICESat-2, Sentinel-1 and Sentinel-2 data using random forest algorithm in Northwest Himalayan foothills of India," *Geophys. Res. Lett.*, vol. 48, no. e2021GL093799, Jul. 2021, doi: 10.1029/2021GL093799.
[39] C. A. Silva et al., "Fusing simulated GEDI, ICESat-2 and NISAR data for regional aboveground biomass mapping," *Remote Sens. Environ.*, vol. 253, Feb. 2021, Art. no. 112234.
[40] L. Narine, L. Malambo, and S. Popescu, "Characterizing canopy cover with ICESat-2: A case study of southern forests in Texas and Alabama, USA," *Remote Sens. Environ.*, vol. 281, Nov. 2022, Art. no. 113242.
[41] H. Tang et al., "Deriving and validating leaf area index (LAI) at multiple spatial scales through LiDAR remote sensing: A case study in sierra national forest, CA," *Remote Sens. Environ.*, vol. 143, pp. 131–141, Mar. 2014.
[42] R. Hu, G. Yan, X. Mu, and J. Luo, "Indirect measurement of leaf area index on the basis of path length distribution," *Remote Sens. Environ.*, vol. 155, pp. 239–247, Dec. 2014.
[43] D. Guo et al., "Exploring photon-counting laser altimeter ICESat-2 in retrieving LAI and correcting clumping effect," *IEEE Trans. Geosci. Remote Sens.*, vol. 61, 2023, Art. no. 5700409.
[44] S. C. Popescu et al., "Photon counting LiDAR: An adaptive ground and canopy height retrieval algorithm for ICESat-2 data," *Remote Sens. Environ.*, vol. 208, pp. 154–170, Apr. 2018.
[45] A. L. Neuenschwander and L. A. Magruder, "Canopy and terrain height retrievals with ICESat-2: A first look," *Remote Sens.*, vol. 11, no. 14, p. 1721, Jul. 2019.
[46] Y. Wang and H. Fang, "Estimation of LAI with the LiDAR technology: A review," *Remote Sens.*, vol. 12, no. 20, p. 3457, Oct. 2020.
[47] A. Neuenschwander and K. Pitts, "The ATL08 land and vegetation product for the ICESat-2 mission," *Remote Sens. Environ.*, vol. 221, pp. 247–259, Feb. 2019.
[48] T. Feng et al., "A systematic evaluation of multi-resolution ICESat-2 ATL08 terrain and canopy heights in boreal forests," *Remote Sens. Environ.*, vol. 291, Jun. 2023, Art. no. 113570.
[49] A. Neuenschwander and K. Pitts, "Ice, cloud, and land elevation Satellite-2 (ICESat-2) algorithm theoretical basis document (ATBD) for land-vegetation along-track products (ATL08)," NASA Goddard Space Flight Center, Greenbelt, MD, USA, Tech. Rep. Release 004, 2021.
[50] A. L. Neuenschwander et al., "ATLAS/ICESat-2 L3A land and vegetation height, version 5," NASA National Snow and Ice Data Center Distributed Active Archive Center, Boulder, CO, USA, Tech. Rep. Version 5(V005), 2021.
[51] Y. Hwang et al., "Correction for light scattering combined with sub-pixel classification improves estimation of gap fraction from digital cover photography," *Agricult. Forest Meteorol.*, vol. 222, pp. 32–44, May 2016.
[52] X. Zhang, L. Liu, X. Chen, Y. Gao, S. Xie, and J. Mi, "GLC_FCS30: Global land-cover product with fine classification system at 30 m using time-series Landsat imagery," *Earth Syst. Sci. Data*, vol. 13, no. 6, pp. 2753–2776, Jun. 2021.
[53] H. Ma and S. Liang, "Development of the GLASS 250-m leaf area index product (version 6) from MODIS data using the bidirectional LSTM deep learning model," *Remote Sens. Environ.*, vol. 273, May 2022, Art. no. 112985.
[54] J. M. Chen, C. H. Menges, and S. G. Leblanc, "Global mapping of foliage clumping index using multi-angular satellite data," *Remote Sens. Environ.*, vol. 97, no. 4, pp. 447–457, Sep. 2005.
[55] J. Zhang et al., "Leaf area index retrieval with ICESat-2 photon counting LiDAR," *Int. J. Appl. Earth Observ. Geoinf.*, vol. 103, Dec. 2021, Art. no. 102488.
[56] Q. Guo et al., "LiDAR boosts 3D ecological observations and modelings: A review and perspective," *IEEE Geosci. Remote Sens. Mag.*, vol. 9, no. 1, pp. 232–257, Mar. 2021.
[57] H. Fang, F. Baret, S. Plummer, and G. Schaepman-Strub, "An overview of global leaf area index (LAI): Methods, products, validation, and applications," *Rev. Geophys.*, vol. 57, no. 3, pp. 739–799, Sep. 2019.
[58] G. Camps-Valls et al., "A unified vegetation index for quantifying the terrestrial biosphere," *Sci. Adv.*, vol. 7, no. 9, Feb. 2021, Art. no. eabc7447.
[59] D. Guo et al., "Spatio-temporal variation in leaf area index in the yan mountains over the past 40 years and its relationship to hydrothermal conditions," *Ecolog. Indicators*, vol. 157, Dec. 2023, Art. no. 111291.
[60] L. L. Narine, S. C. Popescu, and L. Malambo, "Synergy of ICESat-2 and Landsat for mapping forest aboveground biomass with deep learning," *Remote Sens.*, vol. 11, no. 12, p. 1503, Jun. 2019.
[61] W. Li, Z. Niu, R. Shang, Y. Qin, L. Wang, and H. Chen, "High-resolution mapping of forest canopy height using machine learning by coupling ICESat-2 LiDAR with Sentinel-1, Sentinel-2 and Landsat-8 data," *Int. J. Appl. Earth Observ. Geoinf.*, vol. 92, Oct. 2020, Art. no. 102163.
[62] X. Zhu, C. Wang, S. Nie, F. Pan, X. Xi, and Z. Hu, "Mapping forest height using photon-counting LiDAR data and Landsat 8 OLI data: A case study in Virginia and North Carolina, USA," *Ecol. Indicators*, vol. 114, Jul. 2020, Art. no. 106287.
[63] F. Jiang, F. Zhao, K. Ma, D. Li, and H. Sun, "Mapping the forest canopy height in northern China by synergizing ICESat-2 with Sentinel-2 using a stacking algorithm," *Remote Sens.*, vol. 13, no. 8, p. 1535, Apr. 2021.